Document downloaded from:

http://hdl.handle.net/10251/202391

This paper must be cited as:

Cherpinski, A.; Torres-Giner, S.; Cabedo, L.; Lagaron. Jose M. (2017). Post-processing optimization of electrospun submicron poly(3-hydroxybutyrate) fibers to obtain continuous films of interest in food packaging applications. Food Additives & Contaminants: Part A. 34(10):1817-1830. https://doi.org/10.1080/19440049.2017.1355115

The final publication is available at

https://doi.org/10.1080/19440049.2017.1355115

Copyright Taylor & Francis

Additional Information

Post-processing optimization of electrospun submicron poly(3-hydroxybutyrate) fibers to obtain continuous films of interest in food packaging applications

Adriane Cherpinski[a], Sergio Torres-Giner [a], Luis Cabedo[b] and Jose M. Lagaron[a]

[a]Novel Materials and Nanotechnology Group, Institute of Agrochemistry and Food Technology (IATA), Spanish Council for Scientific Research (CSIC), Calle Catedrático Agustín Escardino Benlloch 7, Paterna, Spain

CONTACT Jose M. Lagaron (lagaron@iata.csic.es)

ABSTRACT

Polyhydroxyalkanoates (PHAs) are one of the most researched family of biodegradable polymers based on renewable materials due to their thermoplastic nature and moisture resistance. The present study was targeted to investigate the preparation and characterization of poly(3-hydroxybutyrate) (PHB) films obtained through the electrospinning technique. To convert them into continuous films and then to increase their application interest in packaging, the electrospun fiber mats were subsequently post-processed by different physical treatments. Thus, the effect of annealing time and cooling method on morphology, molecular order, thermal, optical, mechanical, and barrier properties of the electrospun submicron PHB fibers was studied. Annealing at 160°C, well below the homopolyester melting point, was found to be the minimum temperature at which homogeneous transparent films were produced. The film samples that were cooled slowly after annealing showed the lowest permeability to oxygen, water vapor, and limonene. The optimally post-processed electrospun PHB fibers exhibited similar rigidity to conventional compression-molded PHA films, but with enhanced elongation at break and toughness. Films made by this electrospinning technique have many potential applications, such as in the design of barrier layers, adhesive interlayers, and coatings for fiber- and plastic-based food packaging materials.

KEYWORDS

Barrier properties; coatings; electrospinning; packaging; polyhydroxyalkanoates

Introduction

The use of plastic materials in the food packaging area has been steadily increasing over recent decades due to a number of advantages (cost, versatility, lightness, etc.). However, their extensive use has created some challenges for waste management treatment procedures. In this regard, the use of bio-based and biodegradable polymers has recently received increased attention because of their potential as substitutes for petroleum-based polymers in a broad range of applications (Tharanathan 2003; Shah et al. 2014). The use of bio-based biodegradable and compostable polymers (‘biopolymers’) can lead to improved management of the plastic residues, as well as a reduction in dependency onfossil oil. However, one of the main disadvantages arising from the implementation of biopolymers based on renewable resources is that they present either low barrier performance or strong dependence of physical properties on moisture, which can potentially compromise both food quality and safety. Thus, depending on the application, different material characteristics are needed: for fresh produce, selective gas-permeable materials are essential, while high-barrier materials are needed for oxygensensitive products (Lagaron 2011; Bhardwaj et al. 2014; Rujnić-Sokele and Pilipović 2017).

Among biopolymers, there has been particular interest in the use of polyhydroxyalkanoates (PHAs) (Plackett and Siro 2011). However, the use of PHAs in the plastic industry has been limited by several drawbacks such as the high production costs, brittleness, and low thermal stability in the molten state. One of the most extensively studied biopolymers within the PHA family is poly(3-hydroxybutyrate) (PHB). Its biocompatibility with the human body makes PHB also suitable for a number of biomedical applications (such as implants, surgical plasters, drug delivery systems, and stents) (Yoshiharu 1990; Lee 1996; Hasirci 2000). However, PHB presents low thermal stability, a narrow processing window, a high degree of crystallinity, and high rigidity. PHB possesses an isotactic stereo-regularity that makes it viable to crystallize. However, the low nucleation density of PHB does not allow its efficient crystallization, resulting in the formation of large spherulites (El-Hadi et al. 2002; Weihua et al. 2004). To overcome these drawbacks, copolymerization of 3hydroxybutyrate (3HB) units with 3-hydroxyvalerate (3HV) or 4-hydroxybutyrate (4HB) units to produce poly(3-hydroxybutyrate-co-3-hydroxyvalerate) (PHBV) or poly(3-hydroxybutyrate-co-4-hydroxybutyrate) (P (3HB-co-4HB)), respectively, has been proposed to improve the handling properties of the PHB films (Torres-Giner et al. 2016). Other strategies such as blending with other biopolymers (Avella et al. 1991; Greco and Martuscelli 1989; Avella et al. 1993) or adding nucleating agents (Avella et al. 1993; Withey and Hay 1999) have also been suggested. More recently, melt-spinning and cold-drawing processing technologies have also been reported as strategies to improve, for instance, mechanical properties of PHB articles (Yamamoto et al. 1997; Furuhashi et al. 1998; Gordeyev and Nekrasov 1999).

Electrohydrodynamic processing (EHDP), comprising both electrospinning and electrospraying techniques, is a broadly used and efficient technology for fiber or capsule formation that employs powerful electrical forces to produce highly controlled materials (Chronakis 2010; Echegoyen et al. 2017). It has recently gained much attention not only due to its versatility in processing a wide range of polymer and biopolymer materials, but also because of its ability to produce ultrathin structures of diameters within the submicron range that cannot be achieved using other more conventional technologies (Subbiah et al. 2005). In the literature, there are some reports on the use of electrospun PHA fibers with different purposes (e.g. filtration membranes and catalytic nanofibers) (Frenot and Chronakis 2003; Huang et al. 2003; Subbiah et al. 2005), as well as bioactive applications (e.g. encapsulation of food ingredients, antimicrobial coatings, and systems with sustained-release capacity) (Torres-Giner et al. 2016).

In relation to PHB, composition-graded films (CGF) of fluoroapatite (FAP) and PHB with enhanced mechanical properties, such as tensile strength and extension rate compared with pure PHB, have been reported as an electrospun scaffold material for tissue engineering (Zhao et al. 2007). Flexible polylactide (PLA)/PHB electrospun blends were also developed by means of electrospinning, where PLA was reported to slow down the disintegration process (Arrieta et al. 2015). The properties of nanobiocomposites prepared by solvent casting made of PHBV and poly(ε-caprolactone) (PCL) containing carbon nanofibers (CNFs) or carbon nanotubes (CNTs) as fillers were also reported, where enhanced conductivity, thermal, mechanical, and barrier properties were found (Sanchez-Garcia et al. 2010). Another study reported on blends of starch/PHB where different parameters such as blend proportions, thermal, mechanical properties, and alike were discussed in detail (Lagaron and Lopez-Rubio 2011).

In more direct relation to this study, multilayer systems containing electrospun fibers obtained from zein and pullulan with strong adhesive properties resulting from the high surface-to-volume ratios of the ultrathin fibers obtained were reported to significantly contribute to improve the barrier performance of compression-molded PHA films (Fabra et al. 2013). Multilayers containing postprocessed PHA electrospun fibers were seen to exhibit improved barrier properties and strong interlayer adhesion for wheat gluten (Fabra et al. 2013). The gas and vapor barrier properties of the electrospun interlayers were mainly determined by the morphology, thickness, and inherent barrier of the materials, but also by the thermal post-processing. Annealing below the melting point of the biopolymer leads to fibers coalescence and hence to a homogeneous and continuous film with virtually little or no pososity. However, the full impact

of post-processing has never been studied in detail. Thus, to the best of our knowledge, there is no prior literature reporting on the characterization of PHB monolayer films obtained by electrospinning and more specifically on how annealing, cooling, and orientation of the fibers can affect the ultimate physico-chemical properties of the developed materials. Therefore, the main goal of this paper is to develop and characterize PHB films obtained by electrospinning and to evaluate how the morphology, molecular order, thermal, optical, mechanical, and barrier properties are influenced by the specific processing and post-processing conditions used.

Sample code	Processing time at 160°C (min)	Cooling method	Collector type
t_0	0	Air at room temperature	Static
t_5	5	Air at room temperature	Static
Drum w t_0	0	Water	Drum
Ice t_0	0	Ice	Static
Ice t_5	5	Ice	Static
Water t_0	0	Water	Static
Water t_5	5	Water	Static
Hot-press	0	Cooled slowly inside the hot-press	Static
PHB	–	Compression molding from pellets and cooled at room temperature	–
Fibers	–	–	Static

Sample codification and description of the here-developed electrospun poly(3-hydroxybutyrate) (PHB) materials.

Materials and methods

Materials

Bacterial aliphatic homopolyester PHB was supplied by Biomer (Krailling, Germany) as P226F. According to the manufacturer, this is certified both as compostable and food contact, having a density of 1.25 g/cm^3 and a melt flow rate (MFR) of 10 g/10 min at 180°C and 5 kg. The molecular weight (M_w) estimated by the manufacturer was 500 kDa and the polydispersity index (PI) was 2. 2,2,2trifuoroethanol (TFE) with 99% purity and D-limonene with 98% purity were both purchased from Sigma-Aldrich (Madrid, Spain). All products were used as received without further purification.

Preparation of the films

The electrospinning solutions were prepared by dissolving PHB, under magnetic stirring, in TFE at 10% in weight (wt.-%). These conditions were found to be the most adequate for the formation of stable jets of the biopolymer. Other solvents were screened, but did not provide better results.

The electrospinning device used was a Fluidnatek® LE10 lab line from Bioinicia S.L. (Valencia, Spain) with a scanning injector to obtain a homogeneous deposition of the fibers. Scanning has rarely been used by the scientific community in the past, and is thought not only to provide a more homogeneous deposition of the fibers but also to generate a different, more compact, fiber mesh morphology as compared to conventional static injectors. To obtain the electrospun PHB layers, the biopolymer solution was transferred to a 30-mL plastic syringe and connected through polytetrafluorethylene (PTFE) tubes to a stainless steel needle (diameter 0.9 mm). The solution was electrospun for 3 h under a steady flow-rate of 2 mL/h using a motorized injector, scanning horizontally towards a metallic grid or to a metallic rotating drum, which were used as collectors. The distance between the injector and collector was optimal at 15 cm and the voltage was at 15 kV. All experiments were performed at room conditions – 23°C and 40% RH – in a controlled environmental chamber. As stated above, for fiber orientation, the electrospinning process was carried out in the same conditions but the fibers were deposited on a drum or mandrel collector rotating at 1000 rpm for 3 h. Although different rotating speeds were carried out, clear fiber orientation was only seen beyond 500 rpm

Table 1.

and, additionally, at 1000 rpm a compromise between orientation and fiber collection was found optimal.

Of the different annealing temperatures used (140, 150, 160, and 170°C), 160°C was selected as it was the lowest suitable annealing temperature able to yield transparent continuous films. Thus, for the annealing steps, the films were subjected to a temperature of 160°C by compression molding using a hydraulic press 4122-model from Carver, Inc. (Indiana, USA). Different annealing times and four cooling processes were used. These cooling treatments included: (i) air at room temperature (RT), (ii) water at 25°C, (iii) ice, and (iv) slow cooling without temperature within the hydraulic hot-press until reaching room temperature (25°C). The effect of annealing time was screened in samples cooled in air (0, 5, 10, 15, and 20 min), water (0 and 5 min), and ice (0 and 5 min). Table 1 gathers the samples prepared and the coding used throughout the paper.

Characterization of the films Film thickness

Film thickness was measured with a digital micrometer series S00014, having ±0.001 mm accuracy, from Mitutoyo Corporation (Kawasaki, Japan) at three random positions. Average values were used for water vapor, oxygen, and D-limonene permeability determinations. The post-processed samples had a thickness of typically 30 ± 4 μm.

Water vapor permeability

The water vapor permeability (WVP) of the samples were determined, in triplicate, using the gravimetric method ASTM E96-95 (Standard 1989; Arrieta et al. 2015). To this end, 5 mL of distilled water was placed inside a Payne permeability cup (diameter 3.5 cm) from Elcometer Sprl (Hermallesous-Argenteau, Belgium) to expose the film to 100% RH on one side. The liquid was not in contact with the film. Once the films were secured with silicon rings, they were placed within a desiccator at 0% RH cabinet at 25°C. The dryness of the cabinet was held constant using dried silica gel. Cups with aluminium films were used as control samples to estimate solvent loss through the sealing. The cups were weighted periodically using an analytical balance with a ±0.0001 g accuracy. Water vapor permeation was calculated from the steady-state permeation slopes obtained from the regression analysis of weight loss data versus time, and the weight loss was calculated as the total loss minus the loss through the sealing. The permeability was obtained by multiplying the permeance by the film thickness (Sanchez-Garcia and Lagaron 2010; Lagaron and Lopez-Rubio 2011).

D-limonene permeability

Permeability to limonene vapor was measured as described above for WVP. For this, 5 mL of D-limonene was placed inside the Payne permeability cups. The cups containing the films were placed at controlled conditions of 25°C and 40% RH. Limonene vapor permeation rates were estimated from the steady-state permeation slopes and weight loss was calculated as the total cell loss minus the loss through the sealing. The samples were measured in triplicate and limonene permeability rates were calculated taking into account the average film thickness in each case.

Oxygen permeability

The oxygen permeability coefficient was derived from oxygen transmission rate (OTR) measurements recorded, in duplicate, using an Oxygen Permeation Analyzer M8001 from Systech Illinois (Thame, U.K.) at 80% RH and 25°C. The samples were previously purged with nitrogen in the humidity-equilibrated samples, before exposure to an oxygen flow of 10 mL/min. The exposure area during the test was 5 cm^2 for each sample. In order to obtain the oxygen permeability, film thickness and gas partial pressure were considered.

Scanning electron microscopy

A S-4800 microscope from Hitachi (Tokyo, Japan) was used to observe the morphology of the electrospun PHB films, cross-sections, and surfaces by scanning electron microscopy (SEM). Cross-sections of the samples were prepared by cryofracture of the electrospun PHB films using liquid nitrogen. Then, they were fixed to bevelled holders using conductive double-sided adhesive tape, sputtered with a mixture of gold-palladium under vacuum, and observed using an accelerating voltage of 5 kV.

Differential scanning calorimetry

Thermal analyses of electrospun PHB fibers were carried out by differential scanning calorimetry (DSC) on a DSC-7 analyzer from PerkinElmer, Inc.

(Waltham, MA, U.S.A.). A heating program from −20 to 200°C in a nitrogen atmosphere was used using a refrigerating cooling accessory Intracooler 2 (also from PerkinElmer, Inc.). The scanning rate was 10°C/min to minimize the influence of this parameter in the thermal properties. An empty aluminium cup was used as a reference. Calibration was performed using an indium sample. All tests were carried out, at least, in triplicate.

FTIR spectroscopy

Fourier transform infrared spectroscopy (FTIR) spectra were collected coupling the attenuated total reflection (ATR) accessory Golden Gate of Specac, Ltd (Orpington, U.K.) to Bruker Tensor 37 FTIR equipment (Rheinstetten, Germany). Single spectra were collected in the wavelength range from 4000 to 600 cm^{-1} by averaging 20 scans at a resolution of 4 cm^{-1}.

Optical properties

The transparency of the films was determined through the surface reflectance spectra using a spectrocolorimeter CM-3600d from Minolta Co. (Tokyo, Japan) with a 10-mm illuminated sample area. Measurements were taken in triplicate for each sample by using both a white and a black background. Film transparency was evaluated through the internal transmittance (T_i) in a 0–1 theoretical range by applying the Kubelka–Munk theory for multiple scattering to the reflection, following Equation (1). In this equation, R_0 is the reflectance of the film on an ideal black background. Parameters a and b are calculated from the reflectance of the sample (R) and the layer backed by a known reflectance (Rg) according to Equation (2) and (3), respectively (Hutchings 1999).

$$T_i = \sqrt{(a - R_0)^2 - b^2} \quad (1)$$

$$a = \frac{1}{2}\left(R + \frac{R_0 - R + R_g}{R_0 R_g}\right) \quad (2)$$

$$b = \sqrt{(a^2 - 1)} \quad (3)$$

Mechanical properties

Tensile tests were performed according to ASTM standard method D638 using an Instron 4400 universal testing instrument from Instron (Norwood, MA, U.S.A.). The tests were performed using 115 × 16 mm^2 stamped dumb-bell shaped specimens. The cross-head speed used in the tests was 10 mm/min. The experiments were performed at room conditions of 25°C and 40% RH. All the tests were recorded in quadruplicate.

Statistical analysis

The samples properties were evaluated through analysis of variance (ANOVA) using Statgraphics Plus for Windows 5.1 from Manugistics Corporation (Rockville, MD, U.S.A.). Fisher's least significant difference (LSD) was used at the 95% confidence level ($p < 0.05$). Mean values and standard errors were also calculated.

Results and discussion

Morphology

The morphology of the electrospun fibers before and after the annealing and cooling processes was analyzed by SEM. As expected, significant changes can be discerned in the cross-sectional images before (Figure 1) and after (Figures 2 and 3) the post-processing treatment. Surface and cross-section micrographs gleaned similar information and clearly revealed different morphologies and arrangements. The diameter of the obtained electrospun PHB fibers was found to peak at around 210 nm. The morphology of the annealed PHB films indicates that the starting electrospun non-woven fibers mat morphology is lost due to ultrathin fiber coalescence during the annealing step, leading to a packing of the material into a continuous film with some varying levels of porosity.

For the samples cooled in air at room temperature, an increase in annealing time up to 5 min appeared to induce somewhat more compact or less porous structures as compared to its counterpart annealed but not isothermally treated (t_0). The differences between the non-isothermal treatment (sample t_0) and isothermal treatment for up to 5 min (t_5) at 160°C are, however, relatively small and relate mainly to somewhat lower porosity. Further annealing time also led to compact

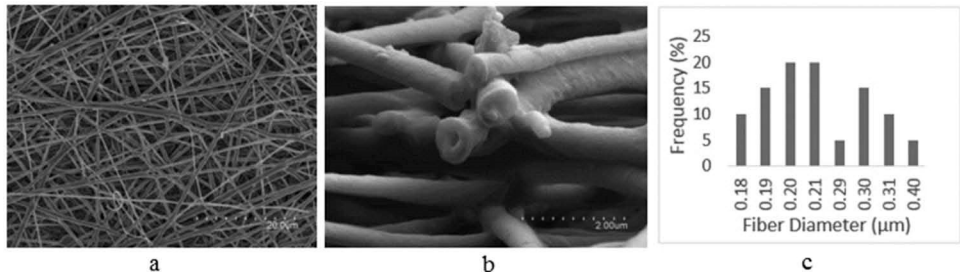

Figure 1. Scanning electron microscopy (SEM) images of the electrospun poly(3-hydroxybutyrate) (PHB) fibers before annealing process at 160ºC: (a) Surface view; (b) Cross-sectional view; (c) Size distribution of fibers.

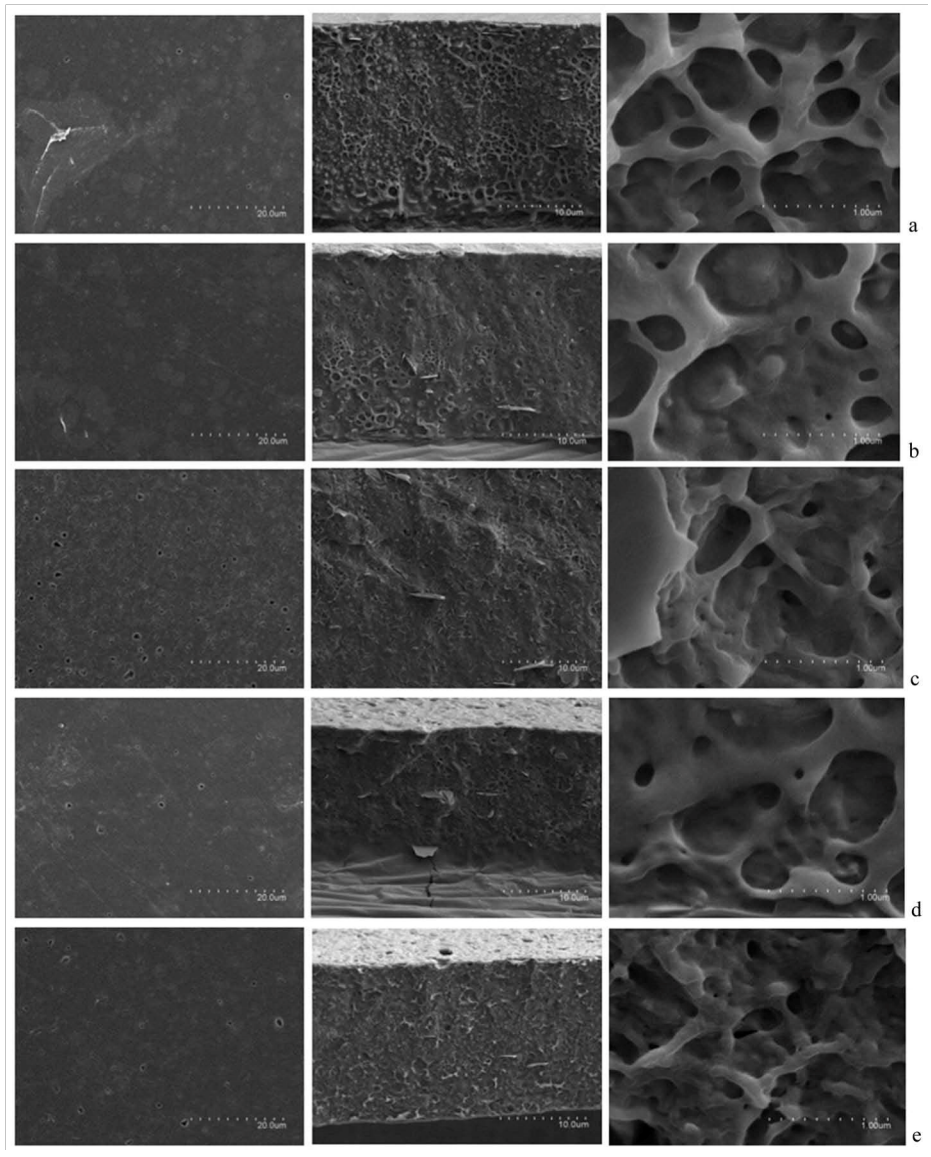

Figure 2. Scanning electron microscopy (SEM) images taken on surface and cross-section of the electrospun poly(3-hydroxybutyrate) (PHB) fibers cooled at room temperature and isothermally post-processed at 160ºC and at different time intervals: (a) 0 min; (b) 5 min; (c) 10 min; (d) 15 min; (e) 20 min.

structures but with somewhat higher porosity; this is more noticeable in the SEM images taken at higher magnification of the samples annealed for 20 min. With increasing annealing time, some yellowing of the samples was also seen. Thus, longer annealing times

seem suboptimal from a morphological and stability viewpoint. In addition to this, due to the very fast film-making processes taking place in the plastics processing industry, long thermal treatments would strongly impair industrial application for this process.

For a given annealing time, no significant differences were encountered among the samples cooled under different conditions (see Figure 3), with the exception of the sample slowly cooled inside the hotpress, which was the one showing the highest compact structure since cooling occurred at a comparatively much slower pace. This sample also appears to exhibit the thinnest cross-section, in accordance with its higher degree of compactness. Despite this, such slow cooling is not a process that could be industrially meaningful. The samples cooled in ice are those with the highest expected cooling rate and, due to there was no isothermal treatment, they exhibited an apparent higher degree of porosity. In order of cooling rate, the samples were graded as follows: ice > water > RT > hot-press.

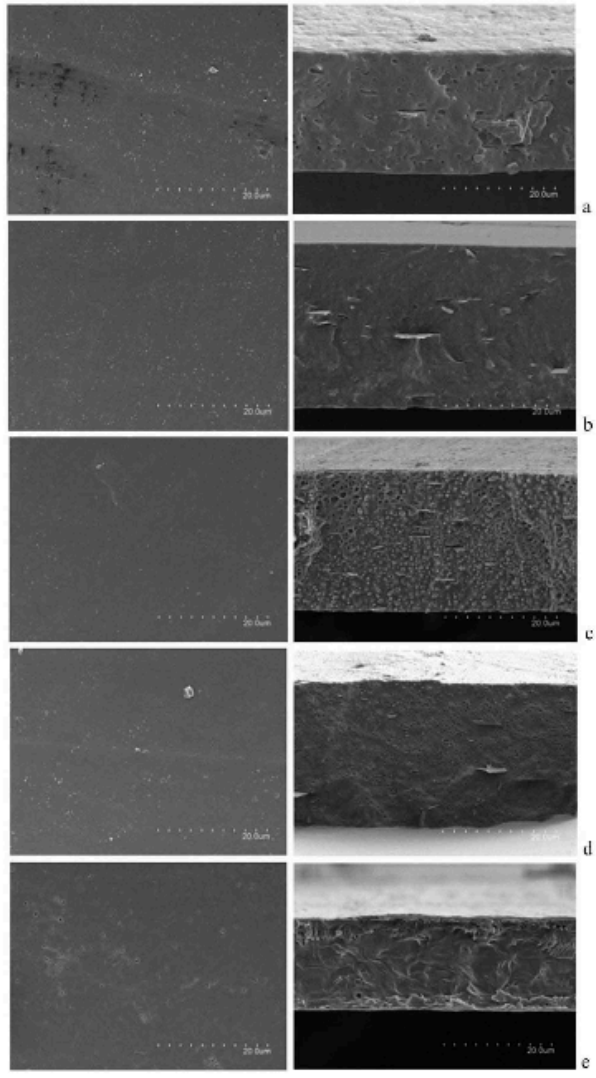

Figure 3. Scanning electron microscopy (SEM) images taken on surface and cross-section of the electrospun poly(3-hydroxybutyrate) (PHB) fibers isothermally post-processed at 160ºC under different conditions: (a) 0 min of annealing and cooling in ice; (b) 5 min of annealing and cooling in ice (c); 0 min of annealing and cooling in water (d); 5 min of annealing and cooling in water; (e) 0 min of annealing and cooled in hot-press.

Chemical analysis

Generally, FTIR spectroscopy is sensitive to the conformational and local molecular environment of chemicals. Therefore, it has been extensively used as a convenient and powerful tool for investigating the chemical structure and conformational changes along the backbone of polymers. Figure 4 shows the FTIR spectra of the samples annealed at different time

intervals of between 0 and 20 min. In these spectra, the strong conformationally sensitive band at 17220 cm^{-1} assigned to C = O stretching vibration of the PHB (Fabra et al. 2013) is clearly visible. Moreover, the C-O-C stretching vibration bands at 1228 and 1278 cm shoulder peaks at 1290 and 1263 cm typical fingerprint vibrations of PHB (Fabra et al. 2013). From observation of the FTIR spectra as a function of time, there are no new features, band shift, or shape changes that could unambiguously suggest chemical alterations by annealing across time. These results are consistent with previous work reported by (Pachekoski et al. 2013), which showed that despite the observed molar mass reduction and increase in melt index during polymer degradation, FTIR was not able to pick up significant band variations. However, closer inspection of Figure 4 reveals that the carbonyl stretching band develops with annealing time an increasing high wavenumbers shoulder. This overall band widening with annealing time is here ascribed to changes in molecular order along the backbone and in turn to crystallinity.

In fact, FTIR has been previously used to estimate crystallinity in PHB. Mottin et al. (2016) concluded that the ratio of the bands A1230:A1453 cm^{-1} was indicative of changes in crystallinity in the sample. Xu et al. (2002) heated a PHB film and collected the FTIR spectra in situ during the heating process, and found that the absorbance ratio of the crystalline band at 1230 cm^{-1} to the reference band at 1453 cm^{-1} was decreasing with decreasing crystallinity. They also found that the carbonyl stretching band was undergoing broadening with decreasing crystallinity. Porter and Yu (2011) suggested that the ratio A1184:A1382 cm^{-1} was also providing an indication of crystallinity changes in PHB. According to their study, the absorption intensity at 1184 cm^{-1} decreases with increasing crystallinity while the 1382 cm^{-1} does not change. The band at 1186 cm^{-1} is assigned to the asymmetric stretching vibration of the C-O-C group,

Table 2. Fourier transform infrared spectroscopy (FTIR) crystallinity assessment from the full width at half maximum (FWHM) of the carbonyl band centered at ~1722 cm^{-1} and the band area ratio A1230:A1453 cm^{-1} for the electrospun poly(3-hydroxybutyrate) (PHB) samples processed with increasing annealing time and cooled in air at room temperature.

Sample	$FWHM_{1722\ cm-1}$	A1230:A1453 cm^{-1}
Fibers	17.50	3.53
t_0	17.29	3.56
t_5	19.71	3.36
t_{10}	20.30	3.57
t_{15}	25.44	3.01
t_{20}	27.00	3.39

while the band at 1382 cm^{-1} is ascribed to the symmetric wagging of the CH_3 groups. Xu et al. (2002) discussed that the latter band ratio was less reliable than A1230: A1453 cm^{-1}, since the band at 1382 cm^{-1} was seen to change during crystallization.

Table 2 shows the full width at half maximum of the carbonyl band at ca. 1722 cm^{-1} and also the ratio A1230:A1453 cm^{-1}. From these indicators, it seems clear that annealing of the fibers leads to widening of the carbonyl band at 1722 cm^{-1}, which is associated with a decrease in crystallinity. Interestingly, the PHB fibers, when annealed at 160°C at t_0, underwent a reproducible narrowing of the band, suggesting some increase in crystallinity, while crystallinity began to reduce with increasing time of the isothermal treatment, especially beyond 10 min. Consistent with the overall behavior of the carbonyl band, the band ratio A1230:A1453 cm^{-1} was seen to go up and then down.

Table 3 summarizes the full width at half maximum of the carbonyl band at ~1722 cm^{-1} and also the band ratio A1230:A1453 cm^{-1}. From the first index, the samples cooled in the hot-press showed the lowest carbonyl band width – suggesting that the highest crystallinity and the fast-cooled samples at t_0 showed the largest values, indicating lower crystallinity. During isothermal exposure for 5 min, crystallinity seems to develop to some extent. A similar trend was provided by the A1230:A1453 cm^{-1} ratio.

Table 3. Fourier transform infrared spectroscopy (FTIR) crystallinity estimation from the full width at half maximum (FWHM) of the carbonyl band centred at ~1722 cm^{-1} and the band area ratio A1230:A1453 cm^{-1} for the electrospun poly(3-

hydroxybutyrate) (PHB) samples processed with different cooling processes.

Sample	FWHM$_{1722\ cm-1}$	A1230:A1453 cm^{-1}
Hot-press	17.00	4.01
Ice t_0	24.29	3.55
Ice t_5	20.38	3.63
Water t_0	22.90	3.28
Water t_5	21.52	3.38

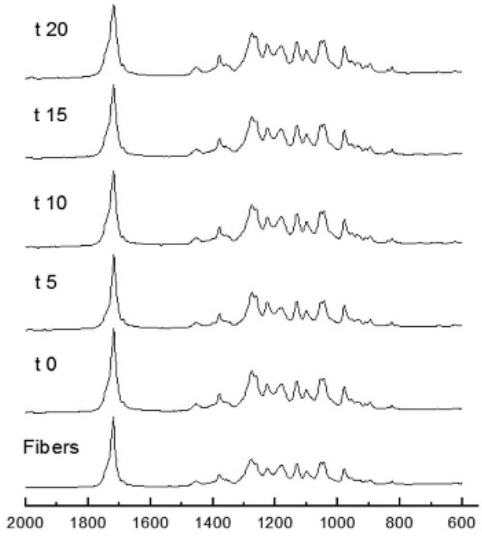

Figure 4. Fourier transform infrared spectroscopy (FTIR) spectra of the electrospun poly(3-hydroxybutyrate) (PHB) fibers mat and of the films annealed for up to 20 min.

Thermal properties

It is clear from the DSC thermograms (Figure 5) that, while the PHB fibers showed two melting features, one at ~50°C related to the melting of a low-molecular-weight additive (typically a plasticizer and another one at ~169°C related to the melting of the PHB crystals), the annealed samples

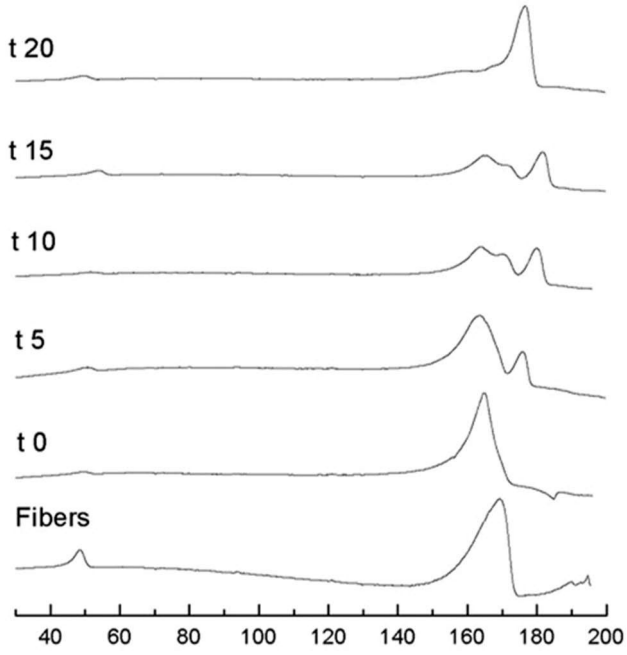

Figure 5. Differential scanning calorimetry (DSC) thermograms of the electrospun poly(3-hydroxybutyrate) (PHB) fibers and of the films with 0–20 min of annealing.

Table 4. Thermal properties obtained from the differential scanning calorimetry (DSC) curves in terms of melting temperature of the plasticizer (T_{plast}), melting temperature (T_m), normalized melting enthalpy (ΔH_m), crystallization temperature (T_c), and crystallization enthalpies (ΔH_c) for the various poly(3-hydroxybutyrate) (PHB) samples.

Sample	$Tm_{plast.}$	Tm_1 (ºC)	Tm_2 (ºC)	ΔHm (J/g)	Tc(ºC)	ΔHc (J/g)
PHB	46.7 (0.7)^{ab}	169.4 (0.2)^{a}	–	76.8 (0.4)^{c}	110.3 (0.3)^{a}	64.0 (0.4)^{c}
Fibers	47.5 (0.2)^{ab}	169.3 (0.1)^{a}	–	64.2 (1.6)^{a}	110.4 (0.7)^{a}	59.5 (0.5)^{ab}
t_0	48.7 (0.7)^{ab}	165.8 (1.3)^{b}	–	71.9 (2.4)^{b}	110.6 (0.7)^{c}	61.1 (0.3)^{a}
t_5	46.5 (0.6)^{ab}	163.5 (0.2)^{bc}	175.8 (1.2)^{a}	81.2 (1.4)^{c}	110.0 (0.3)^{c}	60.0 (1.7)^{a}
t_{10}	50.4 (1.2)^{a}	162.2 (1.6)^{c}	177.3 (0.3)^{a}	78.4 (0.8)^{c}	110.4 (1.0)^{a}	60.8 (1.4)^{a}
t_{15}	48.7 (0.3)^{ab}	161.5 (1.0)^{c}	176.9 (0.3)^{a}	80.4 (1.9)^{c}	109.6 (2.2)^{a}	59.5 (1.7)^{a}
t_{20}	47.0 (0.9)^{ab}	176.5 (0.2)^{d}	–	80.7 (0.6)^{c}	109.7 (0.1)^{a}	57.8 (0.6)^{b}

Mean value (standard error).

a–d: Different superscripts within the same column indicate significant differences among samples ($p < 0.05$).

show a more complex melting behavior with multiple melting endotherms, which are ascribed in PHB to melting and recrystallization during the DSC runs. This makes it difficult to determine the actual sample crystallinity or a single melting point from the technique, since these develop over the run (Martínez-Abad et al. 2016). Table 4 gathers the melting points, melting enthalpies, crystallization temperatures, and crystallization enthalpies for the sample compression molded, for the fibers, and for the annealed films at various times. From this, it seems that with increasing annealing time the crystallization temperature tends to decrease somewhat (especially in the samples processed with 15 and 20 min of annealing), as well as the crystallization enthalpy. This could indicate that these long-time annealed samples could develop some impairments for crystallization – perhaps due to partial degradation, consistent with the FTIR data and some light color development.

Since the samples annealed for longer than 5 min did not yield a better morphology or even crystallinity and, furthermore, are not expected to meet current industrial processes, the rest of the characterization was carried out only on samples cooled under different conditions and annealed either at t_0 or at t_5. Of these, the samples annealed at t_0 and cooled in air at RT are the ones that could show more potential applicability in the packaging industry, since they could be applied to existing lamination and curing machinery.

Table 5 summarizes the thermal data for the samples cooled using different methods, and for the sample collected on a rotating mandrel. These data demonstrate that the sample slowly cooled in the hot-press showed the highest melting temperature and enthalpy, as would be expected. These enhanced melting data could also correlate with a more pronounced melting recrystallization process during the DSC run, since the PHB sample was allowed to cool very slowly and so could also develop crystallinity more easily.

Table 5. Thermal properties obtained from the differential scanning calorimetry (DSC) curves in terms of melting temperature of the plasticizer (T_{plast}), melting temperature (T_m), normalized melting enthalpy (ΔH_m), crystallization temperature (T_c), and crystallization enthalpies (ΔH_c) for the electrospun poly(3-hydroxybutyrate) (PHB) samples cooled under different conditions.

Sample	$Tm_{plast.}$	Tm (ºC)	ΔHm (J/g)	Tc(ºC)	ΔHc (J/g)
Ice t_0	44.1 (0.2)^{d}	166.3 (0.3)^{ab}	65.5 (1.1)^{a}	110.9 (0.8)^{ab}	60.5 (0.6)^{a}
Water t_0	49.8 (0.1)^{a}	166.8 (0.2)^{c}	68.4 (0.6)^{c}	111.6 (0.6)^{a}	58.4 (0.3)^{c}
Hot-press t_0	50.3 (0.3)^{b}	175.3 (0.7)^{d}	78.6 (1.9)^{d}	110.2 (0.1)^{a}	61.3 (0.8)^{b}
Drum t_0	49.0 (2.1)^{a}	168.1 (1.4)^{b}	61.7 (2.1)^{b}	110.6 (1.1)^{a}	61.1 (0.1)^{b}

Mean value (standard error).

a–d: Different superscripts within the same column indicate significant differences among samples ($p < 0.05$).

Optical properties

The contact transparency images of the developed films prepared by annealing at the chosen temperature of 160°C and at two different time intervals are shown as an example in Figure 6. The samples annealed at t_0 and t_5 – A and B, respectively – exhibit similar contact transparency. All the annealed materials for up to 5 min presented good contact transparency, which seemed be unaffected by annealing time, suggesting that PHB was not so strongly degraded after 5 min of the mild thermal

Figure 6. Contact transparency of the poly(3-hydroxybutyrate) (PHB) films prepared at various annealing times for up to 5 min and cooled in air at room temperature: (A) t_0; (B) t_5; (C) Compressionmolded PHB film; (D) Electrospun PHB fibers without heat treatment (opaque material, D letter underneath not discernible).

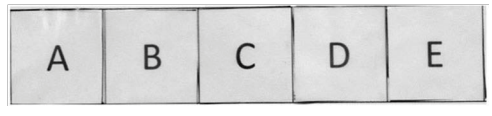

Figure 7. Contact transparency of the poly(3-hydroxybutyrate) (PHB) films prepared at different annealing times and cooled under different conditions. (A) Ice t_0; (B) Ice t_5; (C) Water t_0; (D) Water t_5; (E) Hot-press t_0.

treatment given to the electrospun fibers. By comparison to sample C, which is a compression-molded film of similar thickness, it clearly showed somewhat lower transparency, probably due to somewhat higher crystallinity (see crystallization enthalpy data in Table 4) but perhaps also due to the different sample preparation method where comparatively little thermal exposure is given to the samples. Sample D, which corresponds to the electrospun PHB fibers, was completely opaque – as expected, since the electrospun ultrathin fibers, close to the nano range, are known to refract the light very strongly.

Similarly, Figure 7 shows the contact transparency for the annealed electrospun PHB fibers cooled at different cooling conditions such as cooled by direct immersion in water at room temperature, cooled by direct immersion in ice, and slow-cooled in air. From the results, it is evident that all the samples remained highly transparent, which suggests that the different cooling conditions applied did not apparently alter the optical appearance of the post-processed PHB fibers. These results are further supported by the internal transmittance (T_i) data described below.

It is a well-established fact that post-processing strongly affects the optical behavior of electrospun fibrous materials (Fabra et al. 2013). In general, opacity can be quantitatively assessed in terms of internal transmittance (T_i). Figure 8 describes the absorption properties of the short-time annealed PHB films. A higher value of T_i corresponds to a more transparent film, which indicates a more homogeneous refractive index. On the other hand, a lower T_i value indicates that PHB

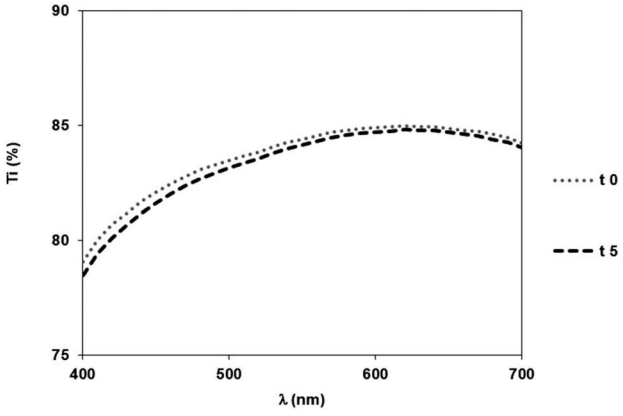

Figure 8. Spectral distribution of internal transmittance for the poly(3-hydroxybutyrate) (PHB) samples at t_0 and t_5.

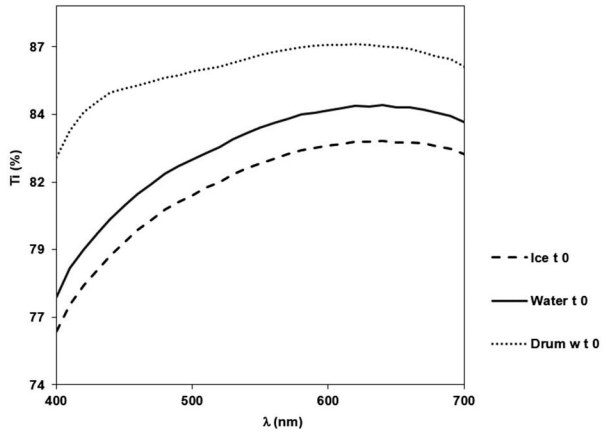

Figure 9. Spectral distribution of internal transmittance for the poly(3-hydroxybutyrate) (PHB) samples cooled in ice t_0, water t_0, and drum w t_0.

films are less transparent, due to their more heterogeneous morphology. As shown in Figure 8, the spectrograph indicates that both samples showed almost the same transmittance, both ranging from 79% to 84%, the sample at t_0 being slightly more transparent.

Figure 9 shows similar patterns for all the postprocessed PHB samples subjected to different cooling conditions. This indicates some differences in their transmittance values, which had a maximum range of 83–87%, again suggesting the highly transparent nature of the samples generated. It seems that the sample cooled in water showed slightly higher transparency. Figure 9 also demonstrates that the PHB samples collected on the rotating drum showed somewhat higher transparency after post-processing – perhaps because the fibers deposited are aligned, thus generating a more homogeneous film after annealing.

Table 6. Mechanical properties in terms of tensile modulus (E), tensile strength at break (σ_b), elongation at break (ε_b), and toughness (T), derived from tensile test of various electrospun poly(3-hydroxybutyrate) (PHB) samples.

Sample	E (MPa)	σ_b (MPa)	ε_b (%)	T (mJ/m^3)
PHB film	1104 (74)^a	17.8 (1.8)^b	2.9 (1.0)^c	0.3 (0.1)^b
t_0	1080 (145)^a	17.3 (5.1)^b	4.5 (1.0)^a	0.6 (0.2)^a
Water t_0	1135 (243)^a	13.4 (1.6)^c	3.9 (2.0)^b	0.4 (0.3)^b
Drum w t_0	1171 (68)^b	20.7 (4.7)^a	3.8 (1.0)^b	0.6 (0.2)^a

Mean value (standard error). a–c: Different superscripts within the same column indicate significant differences among samples ($p < 0.05$).

Mechanical properties

Table 6 presents the results from the tensile tests carried out in some of the most relevant materials. Analysis of these data shows that the storage modulus and tensile strength were only somewhat higher for the oriented PHB sample as compared to the non-oriented fibers and the conventional compression-molding process. This indicates that alignment of the fibers during electrospinning does result in improved rigidity for the system, even when a similar post-processing annealing step was carried out. It is also relevant to observe that the annealed electrospun fibers exhibit an increased elongation at break, as well as toughness, compared with the PHB film. This is significant from an application viewpoint, because PHB is often considered a highly fragile material. By processing the material through electrospinning and post-processing in a controlled manner, a more balance mechanical performance is achieved whereby rigidity is retained but toughness is increased.

Barrier properties

To evaluate how the processing and post-processing parameters – and, hence, the different molecular architecture of the samples – affected the barrier properties of the developed PHB films, water, limonene, and oxygen permeability were finally measured in the most relevant samples. The barrier performance is, in fact, one of the main parameters of application interest in packaging. Table 7 summarizes the WVP values of the developed PHB films. The first observation is that the electrospun PHB films showed somewhat higher WVP values than a compression-molded PHB film: 1.7 10^{-15} kg·m/s·m2·Pa, as measured in our lab previously and reported by Sanchez-Garcia et al. (2007). This could be explained by the fiber network exhibiting some degree of porosity formed during the electrospinning process, but it may also be related to differences in molecular order. However, the samples with the lowest cooling rate – those cooled inside the hotpress or cooled at room temperature and annealed for 5 min – came closer to the reported value in a compression-molded PHB film. These observations suggest that by optimal post-processing of an electrospun fiber-based sample, the material goes from the very low permeability of the fibers mat to a barrier performance close to a film prepared in a conventional industrial process obtained by compression molding (Sanchez-Garcia et al. 2007; Mottin et al. 2016). Thus, electrospun PHB films, which underwent slow cooling in the hot-press, showed the lowest values of WVP as stated above. Table 7 also shows that higher annealing times after fast cooling resulted in a lower barrier, which is in line with the less favorable morphology and lower molecular order, i.e. lower free volume, observed in these samples.

Table 7. Values of water vapor permeability (WVP) of various electrospun poly(3-hydroxybutyrate) (PHB) samples.

Sample	WVP × 10^{15} (kg·m·m^{-2}· Pa^{-1}·s^{-1})
t_0	5.22 (0.40)^{c}
t_5	2.01 (0.30)^{f}
Ice t_0	8.96 (1.20)^{a}
Ice t_5	2.39 (0.80)^{e}
Water t_0	6.92 (0.60)^{b}
Water t_5	3.46 (0.50)^{d}
Hot-press w t_0	1.75 (0.50)^{g}

Mean value (standard error). a–g: Different superscripts within the same column indicate significant differences among samples ($p < 0.05$).

Table 8 shows the D-limonene permeability values of the most relevant samples. Limonene transport properties are important because this component is usually used as a standard system to test aroma barrier. It is also relevant to note that limo-

Table 8. Values of limonene permeability of various electrospun poly(3-hydroxybutyrate) (PHB) samples.

Sample	Limonene permeability × 10^{15} (kg·m·m^{-2}· Pa^{-1}·s^{-1})
t_0	3.20 (0.40)^{f}
t_5	3.93 (0.30)^{b}
Ice t_0	3.31 (1.30)^{e}
Ice t_5	3.83 (0.70)^{c}
Water t_0	4.18 (0.60)^{a}
Water t_5	3.72 (1.20)^{d}
Hot-press w t_0	1.95 (0.10)^{g}

Mean value (standard error). a–g: Different superscripts within the same column indicate significant differences among samples ($p < 0.05$).

Table 9. Values of oxygen permeability of various poly(3hydroxybutyrate) (PHB) samples.

Sample	Oxygen permeability × 10^{14} ($m^3 \cdot m \cdot m^2 \cdot s^{-1}$ Pa^{-1})
PHB film	2.00 (0.10)^c
Water t_0	4.00 (0.30)^a
Water t_5	3.00 (0.30)^b

Mean value (standard error). a–c: Different superscripts within the same column indicate significant differences among samples ($p < 0.05$).

nene, as opposed to moisture, is a strong plasticizer for PHA materials (Sanchez-Garcia et al. 2007). Table 8 indicates that no significant differences were observed between the samples probably due to plasticization, although the sample prepared by slow cooling, i.e. hot-press, showed the lowest values of limonene permeability in line with the higher molecular order inferred for these samples. Sanchez-Garcia et al. (2007) reported that limonene permeability for a similar compression-molded PHB sample was at 8.8×10^{-15} $kg \cdot m/s \cdot m^2 \cdot Pa$. The latter result is somewhat higher than the ones measured in the present study, suggesting that plasticization may occur differently in the electrospun samples. Thus, post-processing interfiber coalescence may create many interphases between the ultrathin fibers, and this could affect the mass transport along this material.

Finally, Table 9 shows the oxygen permeability measured for the PHB film and for the electrospun samples annealed and cooled in water. Oxygen is a non-condensable small gas molecule and, hence, it is more sensitive to the material free volume, defects, and porosity. Thus, the lowest permeability was found for the continuous compression-molded PHB film. The sample annealed for a longer time of 5 min showed somewhat lower permeability, as expected given the enhanced sample compactness and molecular order.

Conclusions

This study showed that novel films with variable properties can be obtained by optimizing the postprocessing conditions of electrospun fibers of PHB – annealing temperature, isothermal time, and cooling rate. The electrospun films showed better optical properties than films of the same thickness processed by conventional compression molding. In general, more compact morphologies and improved properties in terms of barrier performance were found for samples where slow cooling occurred from the isothermal annealing post-processing step at 160°C. FTIR spectroscopy was found to be a non-dynamic adequate method, compared with the conventional dynamic DSC method, to assess molecular order in the materials and correlated fairly well with their barrier performance. The mechanical properties of this type of electrospun films resulted in higher elongation at break and toughness in comparison with their corresponding compression-molded counterparts. Barrier properties were generally found to depend mostly on annealing time but, more importantly, on cooling rate. The results of this study show a very promising new plastic processing technology – the annealed electrospun films – to provide new valorizing forms of processing renewable polymers as interlayers or coatings with enhanced flexibility and transparency while potentially retaining the barrier performance to gases and vapors of the conventional compression-molded films.

In addition, since these materials made of postprocessed submicron electrospun fibers are known to exhibit self-adhesive properties, they offer potential as functional elements in packaging materials made of biopolymers. This is relevant since in the biopolymers field, there is a lack of functional biobased adhesives that can help constitute fully biobased multilayers by acting as tie layers, for use not only in packaging but also as hydrophobic coatings for fiber-based packaging. Finally, since these materials can easily incorporate active or/and bioactive packaging ingredients within the fiber structure, they can potentially be used in the design of active and bioactive packaging strategies requiring controlled release of the active/bioactive ingredients.

Disclosure statement

No potential conflict of interest was reported by the authors.

Funding

This work was supported by the Spanish Ministry of Economy and Competitiveness (MINECO) [Project AGL2015-63855-

C21-R] and by the Brazilian Council for Scientific and Technological Development (CNPq) [Grant 205955/2014-2].

References

Arrieta MP, López J, López D, Kenny JM, Peponi L. 2015. Development of flexible materials based on plasticized electrospun PLA–PHB blends: structural, thermal, mechanical and disintegration properties. Eur Polym J. 73:433–446.

Avella M, Martuscelli E, Greco P. 1991. Crystallization behaviour of poly(ethylene oxide) from poly(3-hydroxybutyrate)/poly(ethylene oxide) blends: phase structuring, morphology and thermal behaviour. Polymer. 32:1647– 1653.

Avella M, Martuscelli E, Raimo M. 1993. The fractionated crystallization phenomenon in poly(3-hydroxybutyrate)/ poly(ethylene oxide) blends. Polymer. 34:3234–3240.

Bhardwaj U, Dhar P, Kumar A, Katiyar V. 2014. Polyhydroxyalkanoates (PHA)-cellulose based nanobiocomposites for food packaging applications. In: Komolprasert V, Turowski P, editors. Food additives and packaging. Washington (DC): ACS Publications; p. 275–314.

Chronakis IS. 2010. Micro-/Nano-Fibers by electrospinning technology: processing, properties and applications. In: Qin L, editor.. Micro-manufacturing engineering and technology. Oxford (UK): William Andrew; p. 264–286.

Echegoyen Y, Fabra M, Castro-Mayorga J, Cherpinski A, Lagaron J. 2017. High throughput electro-hydrodynamic processing in food encapsulation and food packaging applications: viewpoint. Trends Food Sci Technol. 60:71–79.

El-Hadi A, Schnabel R, Straube E, Muller G, Riemschneider M. 2002. Effect of melt processing on crystallization behavior and rheology of poly (3-hydroxybutyrate)(PHB) and its blends. Macromol Mater Eng. 287:363–372.

Fabra MJ, Lopez-Rubio A, Lagaron JM. 2013. High barrier polyhydroxyalcanoate food packaging film by means of nanostructured electrospun interlayers of zein. Food Hydrocoll. 32:106–114.

Frenot A, Chronakis IS. 2003. Polymer nanofibers assembled by electrospinning. Curr Opin Colloid Interface Sci. 8:64–75.

Furuhashi Y, Ito H, Kikutani T, Yamamoto T, Kimizu M, Cakmak M. 1998. Structural analysis of poly (3-hydroxybutyrate-co-3-hydroxyvalerate) fibers prepared by drawing and annealing processes. J Polymer Sci B: Polymer Phys. 36:2471–2482.

Gordeyev S, Nekrasov YP. 1999. Processing and mechanical properties of oriented poly (β-hydroxybutyrate) fibers. J Mater Sci Lett. 18:1691–1692.

Greco P, Martuscelli E. 1989. Crystallization and thermal behaviour of poly (d (—)-3-hydroxybutyrate)-based blends. Polymer. 30:1475–1483.

Hasirci V. 2000. Biodegradable biomedical polymers. Review of degradation of and in vivo responses to polylactides and polyhydroxyalkanoates. New York (NY): Marcel Dekker.

Huang Z-M, Zhang Y-Z, Kotaki M, Ramakrishna S. 2003. A review on polymer nanofibers by electrospinning and their applications in nanocomposites. Compos Sci Technol. 63:2223–2253.

Hutchings JB. 1999. Food and colour appearance. 2nd ed. Gaithersburg (MD): Chapman and Hall Food Science Book, Aspen Publication.

Lagaron J. 2011. (Editor) Multifunctional and nanoreinforced polymers for food packaging. Cambridge (UK): Woodhead Publishing Ltd.

Lagaron JM, Lopez-Rubio A. 2011. Nanotechnology for bioplastics: opportunities, challenges and strategies. Trends in Food Science & Technology. 22:611–617. Lee SY. 1996. Bacterial polyhydroxyalkanoates. Biotechnol Bioeng. 49:1–14.

Martínez-Abad A, Cabedo L, Oliveira CS, Hilliou L, Reis M, Lagarón JM. 2016. Characterization of polyhydroxyalkanoate blends incorporating unpurified biosustainably produced poly (3-hydroxybutyrate-co-3-hydroxyvalerate). J Appl Polym Sci. 133:42633.

Mottin AC, Ayres E, Oréfice RL, Câmara JJD. 2016. What changes in poly (3-hydroxybutyrate)(PHB) when processed as electrospun nanofibers or thermo-compression molded film? Mater Res. 19:57–66.

Pachekoski WM, Dalmolin C, Agnelli JAM. 2013. The influence of the industrial processing on the degradation of poly (hidroxybutyrate)-PHB. Mater Res. 16:237–332.

Plackett D, Siro I. 2011. Polyhydroxyalkanoates (PHAs) for food packaging. In: Lagaron JM, editor. Multifunctional and nanoreinforced polymers for food packaging. Cambridge (UK): Woodhead Publishing Ltd; p. 498–526.

Porter M, Yu J. 2011. Crystallization kinetics of poly (3hydroxybutyrate) granules in different environmental conditions. J Biomater Nanobiotechnol. 2:301.

Rujnić-Sokele M, Pilipović A. 2017. Challenges and opportunities of biodegradable plastics: A mini review. Waste Manag Res. 35:132–140.

Sanchez-Garcia M, Gimenez E, Lagaron J. 2007. Novel PET nanocomposites of interest in food packaging applications and comparative barrier performance with biopolyester nanocomposites. J Plast Film Sheeting. 23:133–148.

Sanchez-Garcia M, Lagaron J. 2010. Novel clay-based nanobiocomposites of biopolyesters with synergistic barrier to
UV light, gas, and vapour. J Appl Polym Sci. 118:188–199.

Sanchez-Garcia M, Lagaron J, Hoa S. 2010. Effect of addition of carbon nanofibers and carbon nanotubes on properties of thermoplastic biopolymers. Compos Sci Technol. 70:1095–1105.

Shah AA, Kato S, Shintani N, Kamini NR, Nakajima-Kambe T. 2014. Microbial degradation of aliphatic and aliphaticaromatic co-polyesters. Appl Microbiol Biotechnol. 98:3437. Standard A. 1989. Standard test methods for water vapor transmission of materials. Annual book of ASTM standards Designation E96-E80. 730–739.

Subbiah T, Bhat G, Tock R, Parameswaran S, Ramkumar S. 2005. Electrospinning of nanofibers. J Appl Polym Sci. 96:557–569.

Tharanathan R. 2003. Biodegradable films and composite coatings: past, present and future. Trends Food Sci Technol. 14:71–78.

Torres-Giner S, Montanes N, Boronat T, Quiles-Carrillo L, Balart R. 2016. Melt grafting of sepiolite nanoclay onto poly (3-hydroxybutyrate-co-4-hydroxybutyrate) by reactive extrusion with multi-functional epoxy-based styreneacrylic oligomer. Eur Polym J. 84:693–707.

Torres-Giner S, Pérez-Masiá R, Lagaron JM. 2016. A review on electrospun polymer nanostructures as advanced bioactive platforms. Polymer Eng Sci. 56:500–527.

Weihua K, He Y, Asakawa N, Inoue Y. 2004. Effect of lignin particles as a nucleating agent on crystallization of poly (3hydroxybutyrate). J Appl Polym Sci. 94:2466–2474.

Withey R, Hay J. 1999. The effect of seeding on the crystallisation of poly (hydroxybutyrate), and co-poly (hydroxybutyrate-co-valerate). Polymer. 40:5147–5152.

Xu J, Guo B-H, Yang R, Wu Q, Chen G-Q, Zhang Z-M. 2002. In situ FTIR study on melting and crystallization of polyhydroxyalkanoates. Polymer. 43:6893–6899.

Yamamoto T, Kimizu M, Kikutani T, Furuhashi Y, Cakmak M. 1997. The effect of drawing and annealing conditions on the structure and properties of bacterial poly (3-hydroxybutyrate-co-3 hydroxyvalerate) fibers. Int Polymer Process. 12:29–37.

Yoshiharu D. 1990. Microbial polyesters. New York: VCH; p. 156 pp.

Zhao D, Wang Y, Xu R, Wu G, Zhang L, Yu D, Cui F, Chen D, Tian W. 2007. Composition-graded films of fluoroapatite/PHB fabricated via electrospinning for tissue engineering. J Bioact Compat Polym. 22:379–393.